Volume 1 | Number 1 | Jan 2013 | Pages 1–100

Analyst

www.rsc.org/analyst

ROYAL SOCIETY OF CHEMISTRY

This is an *Accepted Manuscript*, which has been through the Royal Society of Chemistry peer review process and has been accepted for publication.

Accepted Manuscripts are published online shortly after acceptance, before technical editing, formatting and proof reading. Using this free service, authors can make their results available to the community, in citable form, before we publish the edited article. We will replace this *Accepted Manuscript* with the edited and formatted *Advance Article* as soon as it is available.

You can find more information about *Accepted Manuscripts* in the **Information for Authors**.

Please note that technical editing may introduce minor changes to the text and/or graphics, which may alter content. The journal's standard **Terms & Conditions** and the **Ethical guidelines** still apply. In no event shall the Royal Society of Chemistry be held responsible for any errors or omissions in this *Accepted Manuscript* or any consequences arising from the use of any information it contains.

ROYAL SOCIETY OF CHEMISTRY

www.rsc.org/analyst

Journal Name

ARTICLE

Nuclear accumulation of anthracyclines in endothelium studied by bimodal imaging: fluorescence and Raman microscopy

K. Majzner,[a,b] T. Wojcik,[b] E. Szafraniec,[a] M. Lukawska,[c] I. Oszczapowicz,[c] S. Chlopicki,[b,d*] and M. Baranska [a,b*],

Anthracycline antibiotics display genotoxic activity towards cancer cells but their clinical utility is limited by their cardiac and vascular toxicity. The aim of this study was to develop a Raman-based methodology to study the nuclear accumulation of anthracyclines in endothelium. For that purpose bimodal Confocal Raman and fluorescence Imaging was used to monitor a cellular composition changes as a result of anthracycline exposure on endothelial cells (EA.hy 926), and nuclear drug accumulation, respectively. Simultaneously effects of anthracyclines on endothelium viability was investigated by caspases-3 and -7 and MTT assays.

We demonstrated different degree of accumulation in the nucleus of the endothelial cells for doxorubicin (DOX), daunorubicin (DNR), epidoxorubicin (EDOX) and epidaunorubicin (EDNR). Nuclear accumulation of DOX and EDOX was similar however EDNR accumulated in endothelial nuclei at concentrations 10 times higher as compared to DNR. In turn, epimers of DOX or DNR were both consistently less toxic on endothelium as compared to their congeners as evidenced by MTT and caspase assays. In summary, bimodal Raman and fluorescence-based nucleus profiling proves to be a valuable tool to study endothelial toxicity of anthracyclines.

Introduction

In the field of biomedical science it is highly desired to develop innovative imaging techniques to study the uptake and distribution of bioactive substances in a way that does not require any additional labeling or special and complicated sample preparation. In that context, the vibrational microspectroscopy has become a powerful tool for the biomedical applications. Raman appears to be a sensitive and non-invasive imaging methods for the evaluation of chemicals in order to study the processes taking place inside the cells [1–10] or tissues[11–15] without the need a special sample preparation or further labeling. It is also possible to detect small biochemical changes and their distributions at the sub-cellular level.[16–23] Current imaging methods are often limited by an insufficient sensitivity, specificity and spatial resolution. The use of vibrational spectroscopy to the *in vitro* study is based on the exceptional spectroscopic pattern of the analyte, that improves the selectivity and sensitivity. Raman microspectroscopy combined with fluorescence assays allow for investigation of the distribution of selected components of the sample with micron resolution. Additionally, the use of advanced methods of data analysis, i.e. chemometrics allows the observation of changes in the content of many compounds simultaneously, which creates the enormous diagnostic potential. Based on

Raman spectrum and with support of multivariate statistics and chemometrics it is possible to investigate biochemical changes in the single cell induced by pharmacological treatment. Raman spectral imaging represents a potential avenue for probing various cellular processes and monitoring drug-cell interactions including studies on chemotherapeutics. [24–26]

The anthracycline antibiotics such as doxorubicin (DOX) and its epimer (EDOX) are cytotoxic drugs effective in treatment of cancer.[4,5] Pharmacological activity of anthracyclines is related to the inhibition of topoisomerase, that prevents further division and leads to cell death.[6] Anthracyclines, show a strong cardiotoxicity as well as vascular toxicity linked to endothelial cells damage.[7–10] that limit their clinical usefulness[8,10,14] During the last several years, much effort has gone into finding new anthracycline derivative that would prove to be better in action and less cardiotoxic.[27–29] Daunorubicin (DNR), the first anthracycline introduced into clinical use is highly effective in the treatment of leukemias but exhibits pronounced side effects, especially cardiotoxicity. Doxorubicin is a commonly used anthracyclines in treatment of and Hodgkin's lymphoma, as well as cancers of the bladder, breast, stomach, lung, ovaries, thyroid, soft tissue sarcoma, multiple myeloma.[30] In turn, epidoxorubicin (epirubicin, EDOX) represent a second generation analog that has been proposed as an alternative to doxorubicin because of lesser cardiac toxicity.[31] and is primarily used against breast, ovarian,

gastric, lung cancers and lymphomas[30]. Epidaunorubicin is not used clinically.

The only difference between doxorubicin and daunorubicin is that the side chain of DOX terminates with a primary alcohol, whereas that of DNR terminates with a methyl. This minor difference has important consequences on the spectrum of activity and/or toxicity of DOX and DAU. Epidoxorubicin and epidaunorubicin are semisynthetic derivatives of doxorubicin and daunorubicin, respectively obtained by an axial-to-equatorial epimerization of the hydroxyl group at C-4′ in daunosamine (Figure 1).

It have been shown that DNR and DOX form intercalation complexes with DNA, and the interaction site sequences are 5'-GC-3', 5'-CG-3'.[32] Anthracyclines modify the structure of DNA by intercalation complexes, covalent bonds, but also by changes in the structure of the nitrogenous bases.[33–35]

According to the best of our knowledge, only single reports using measurement with Raman[5], surface-enhanced Raman spectroscopy (SERS)[36] or imaging with Atomic Force Microscopy (AFM) have been previously published on the effects of DOX.[33,37] Using these methodologies, a strong impact of the antibiotic on the DNA chain conformation was demonstrated. Interestingly, using AFM technique, it was shown that DOX-DNA interaction seems to have a minor effect if a low concentration of DOX was used, however at higher concentrations of DOX, strands of DNA are tangled and overlap, so that the fibers appear to be more and more aggregated and entangled. A further increase in the concentrations of DOX results in higher disorder and aggregation of the test plasmid until complete DNA strand breakage.[33]

In our recent work we demonstrated that DOX, and even more so daunorubicin, induced a detrimental response of endothelium in clinically relevant concentrations. Furthermore, we suggested that the difference in endothelial toxicity of doxorubicin and daunorubicin may be linked to differences in their nuclear accumulation and DNA damage-triggered response of endothelium.[38]. Therefore, the aim of the present work was to develop a bimodal, Raman and fluorescence-based methodology to study the structure-activity relationship of nuclear accumulation of antracycline in endothelium to understand better the relationship between nuclear accumulation of anthracyclines and their endothelial toxicity.
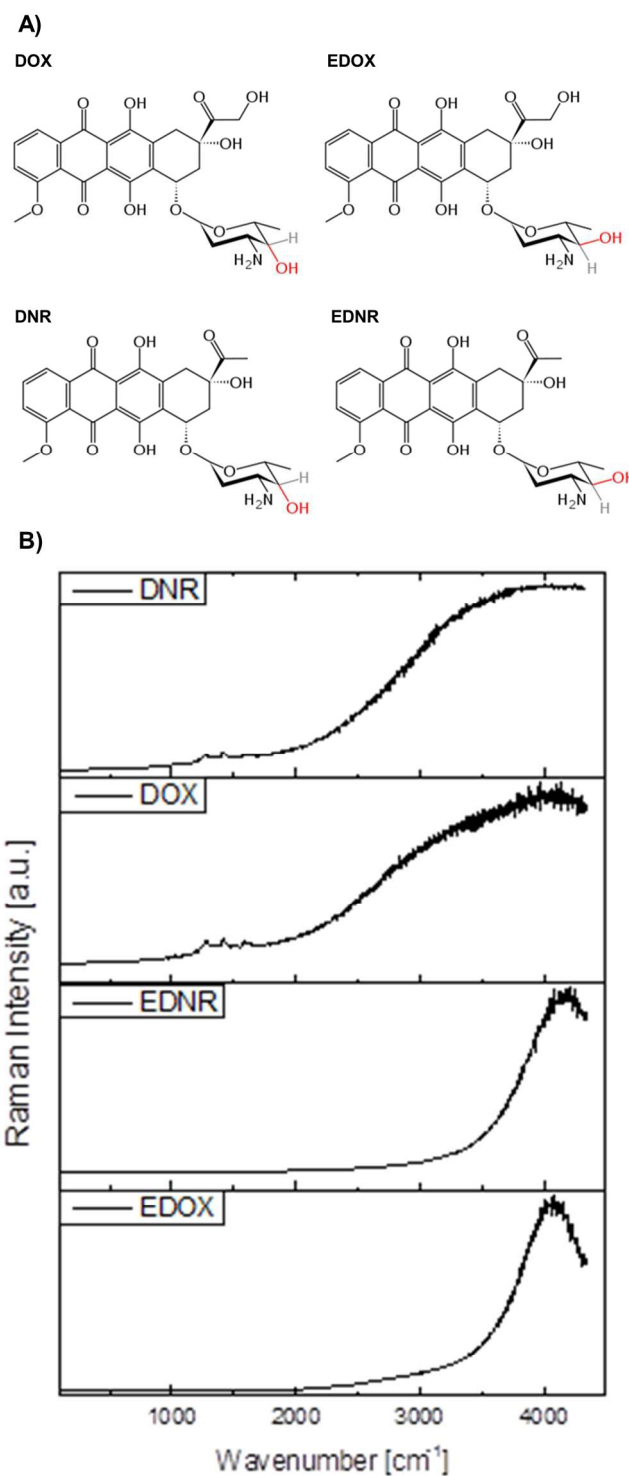
Figure 1 Structures of anthracycline antibiotics: doxorubicin (DOX), epidoxorubicin (EDOX), daunorubicin (DNR), epidaunorubicin (EDNR) and their Raman spectra.

Raman spectra of investigated anthracyclines (Figure 1B) recorded by using 488 nm laser are dominated by the fluorescence. Due to that fact, it was extremely difficult to find a specific Raman band related to changes induced in the cell nuclei. High fluorescence dominated the recorded spectra and

was a reason of low signal-to-noise ratio of the Raman bands. However this enhanced background caused by the fluorescence appears to be a very good marker of the anthracyclines presence in the cells. On the other hand, fluorescence of the anthracycline, despite of the used excitation wavelength, significantly impairs the possibility of observation of resonantly enhanced Raman bands.

Experimental

Cell culture

EA.hy 926 cells, immortalized hybrids, were derived by fusion of Human Umbilical Vein Endothelial Cells (HUVEC) with human lung carcinoma cells line A549. EA.hy 926 cells were cultured at 37°C and 5% CO2 in Dulbecco's modified Eagle's medium (DMEM, Lonza) supplemented with 10% fetal bovine serum (FBS),1% penicillin-streptomycin, 2mM L-Glutamine (Invitrogen) and 2% HAT medium supplement. The cell cultures were incubated in a 37 °C, 5% CO_2/95% air, humidified cell culture incubator and passaged three times a week. For fluorescence microscopy, caspase 3/7 enzyme activity, MTT assay and Electric Cell-substrate Impedance Sensing (ECIS) system experiments cells were plated into 96-well plate at a number of 18 000 per well to produce confluence on the next day post-plating, when exposure to anthracycline was initiated.

Materials

All the tested compounds, with purities > 97.5% according to HPLC method, were obtained from the Institute of Biotechnology and Antibiotics, Warsaw, Poland. Control doxorubicin and daunorubicin were purchased in Sigma-Aldrich Poland.

Raman measurements

For Raman measurements cells (EA.hy926) were cultivated on calcium fluoride slides (CaF_2, 25×2 mm, Pike Technologies, U.S.) placed within wells of 6-well plate, at a number of 5 x 104 per well, and fed with complete medium containing either no anthracycline (control) or a range of concentrations of DOX or DNR (12.5 nM, 25 nM, 50 nm, 300 nM, 500 nM, 1 µM and 10 µM), and EDOX or EDNR (100 nM, 300 nM, 500 nM, 1 µM). After 24 hours the cells were fixed with 2.5% glutaraldehyde (4 min) and stored in isotonic phosphate buffer (pH=7; 4oC), until the start of data acquisition.
Raman mapping was done with a WITec Confocal Raman Microscope (WITec alpha300 R, Ulm, Germany) with the application of a 60× water immersion objective (Nikon Fluor, NA=1). Excitation wavelength of 488 nm was used due to high lateral resolution. A total exposure time was ca. 40-60 min per cell (integration time of 0.7 second per spectrum). Data acquisition was controlled by Witec alpha 300 software package. Pre-processing included cosmic spike removal and background subtraction (using of polynomial fit, order 3) was performed using Witec Project Plus Software. For data exploration the cluster analysis (CA) were implemented. The aim of CA was to group analyzed objects (spectra from the map) into clusters, so that objects (spectra) most similar to each other belong to the same cluster. For the CA, Witec Project

Plus Software was used, based on k – means clustering, Ward's algorithm and Euclidean distance.

High-content fluorescence microscopy

Cells were passaged on 96 well fluorescent imaging plates (Corning, NY, USA), 18 000 per well. The next day cells were treated with anthracyclines in complete medium, for 24 hours. Cells were washed twice with phosphate-buffered saline (PBS), fixed with 2,5% paraformaldehyde (5 minutes) and counterstained with Hoechst 33342 (10 minutes). Images were captured using Olympus Scan^R automated fluorescence microscope in following channels: DAPI for Hoechst 33342 and Cy3 for anthracyclines. All images were stored and processed using Columbus Image Data Storage and Analysis system (Perkin Elmer, Waltham, MA, USA. Nuclear area was identified based on Hoechst 33342 staining. The results for individual cells were presented as means and standard deviations (SD).

Cells viability assay

Cells were passaged on 96 well fluorescent imaging plates (Corning, NY, USA), 18 000 per well. The next day cells were treated with anthracyclines in complete medium, for 24 hours. To each well 100 µl of 0,5 mg/ml 3-(4,5-dimethyl-2-thiazolyl)-2,5-diphenyl-2H-tetrazolium bromide (MTT) in cell medium followed in incubation for 3h at 37 °C. Afterwards, media was carefully removed from the wells after the incubation period. DMSO:ethanol (1:1) was added to each well add the plate was shaked on a plate shaker for 5 min to obtain dye dissolution. The absorbance was measured at 560 nm by a Biotec Synergy 4 plate reader.

Caspases-3 and -7 activity assay

For caspases-3 and -7 activities assay EA.hy926 cells were passaged on white-walled 96-well plates for chemiluminescence measurements (Perkin Elmer). 24 hours post treatment, 200 µl of Caspase Glo 3/7 reagent (Promega, WI, USA) was added to each well and plates were incubated for 3 hours in dark. Luminescence was measured with Synergy 4 plate reader (Biotek, VT, USA). Obtained results were normalized by proteins concentration in samples, calculated based on BCA method.

Wound healing assay with Electric Cell-substrate Impedance Sensing (ECIS)

To examine whether DOX and DNR and their epimers reduce ability of endothelial cells to migration and proliferation, an automated wound healing assay with Electric Cell-substrate Impedance Sensing (ECIS) was applied. EA.hy926 was placed on collagen-coated, stabilized gold film electrodes and cultivated in incubation chamber to confluence. After 12 hours anthracyclines were added in the final concentrations of 200 nM to cells medium. 24 hours later cells were wounded from the electrodes surfaces by high current. The rate of cells migration to wounded area was diminished for cells treated with anthracyclines, in comparison to the control.

Results and discussion

Incubation of endothelial cells with anthracycline resulted in substantial changes in the cell nucleus spectra. The changes were concentration-dependent and occurred as a raised

background in the Raman spectra in the high wavenumber range (3820-4245 cm^{-1}). A comparison of the single spectra from stimulated and control cell was demonstrated in the Figure 2. Similar effect of the background enhancement was observed for all other anthracyclines presented in the Figure 1.
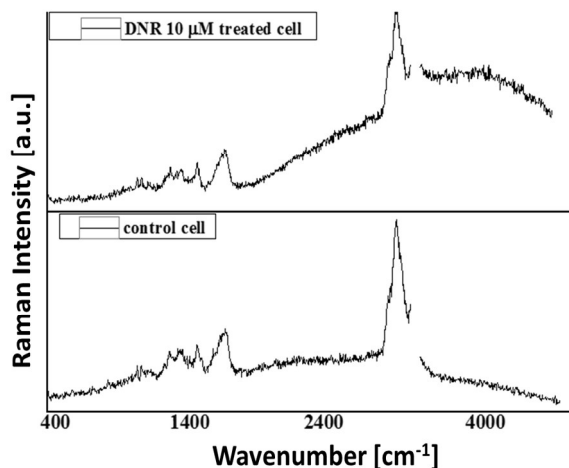

Figure 2 A comparison of single Raman spectra from stimulated (10 µM DNR) and control cell.

Maximum of fluorescence for the anthracycline standards (3820 - 4245 cm^{-1}, data not shown) overlaps with the range, in which the increased background is observed in the Raman spectra from anthracycline-treated cells, therefore this spectral range seems to be a good marker for the presence of anthracycline in the cells. The integration of the Raman spectra obtained from the mapping allows the study of the distribution of the antibiotic in the cell.

In addition, the results obtained for different concentrations of antibiotics help to identify at what concentration the accumulation of anthracyclines in the nucleus was observed. Concentrations below the "threshold concentration" can be regarded as relatively safe for human endothelial cells. Summary of results of typical Raman maps obtained by the integration of in the range of 3820 - 4245 cm^{-1} for DOX and DNR various concentrations is presented in Figure 3. Additionally, to show that observed distribution of accumulated drugs is within the nucleus of cells the integration of 785 cm^{-1} Raman band (due to cytosine ring vibration of DNA) and the integration for 2800–3020 cm^{-1} range (ν_{C-H}) are shown. Figure 3 includes also microphotographs with the marked area of Raman mapping. A comparison of microphotographs and results of integration analysis over ν_{C-H} range shows that in each case the whole area of cell was measured. Results (Figure 3) clearly indicate that DNR in concentrations of 50 nM and higher and DOX in concentrations of 1 µM and higher can be easily detected in the nuclei of cells using Raman microspectroscopy.

A

B
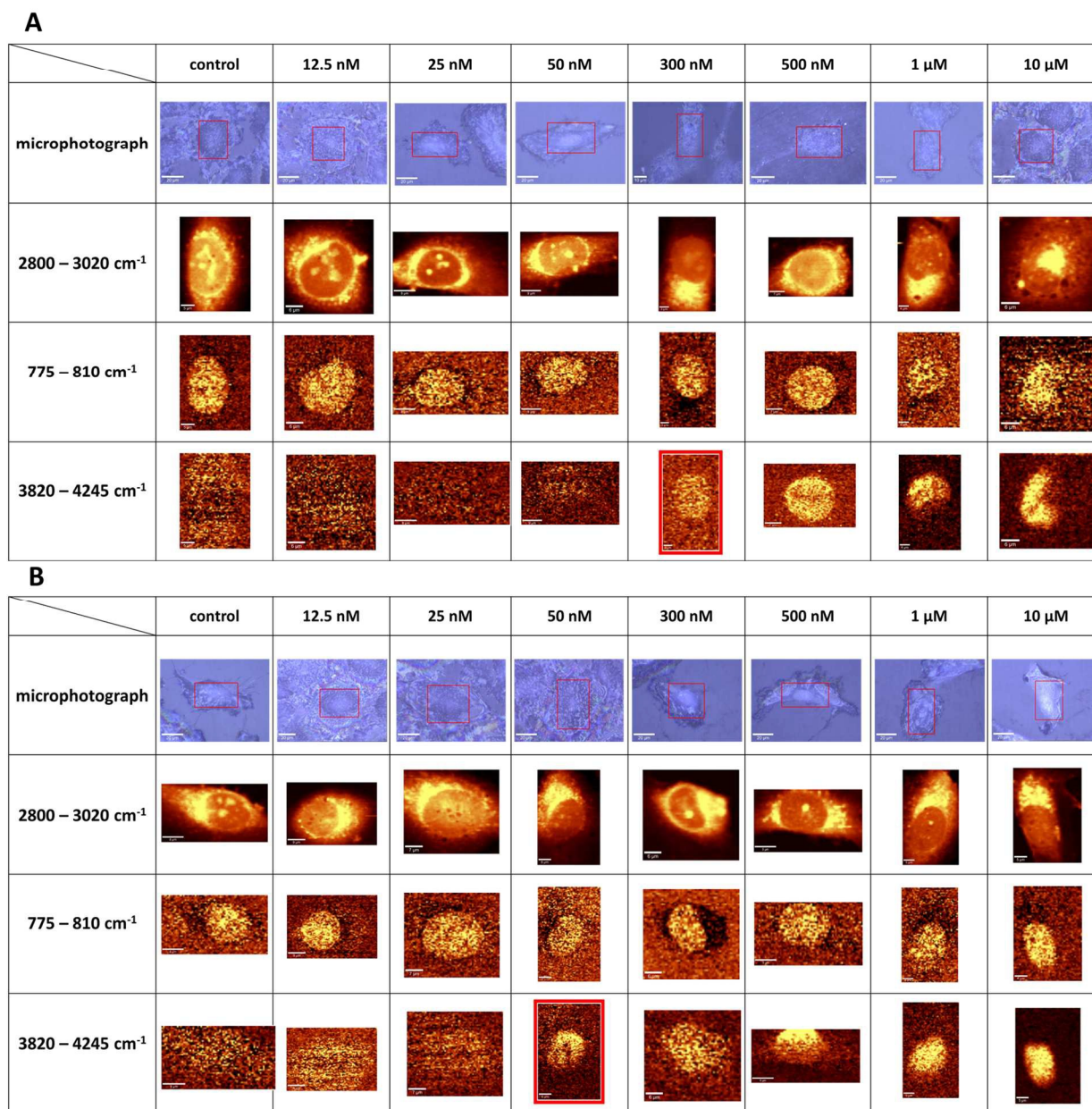
Figure 3 Examples of typical chemical maps obtained by the integration of the Raman spectra over the v_{C-H} band (2800 – 3020 cm^{-1}), cytosine ring vibration of DNA (775–810 cm^{-1}) and 3820-4245 cm^{-1} (spectral range of anthracycline antibiotic maximum fluorescence). A – Integration maps and microphotographs for doxorubicin (DOX), B – integration maps and microphotographs for daunorubicin (DNR). Results for all investigated concentrations of anthracycline antibiotics are shown. "Threshold concentrations" are marked by a red square in the bottom row. Scale bar for bottom row: A) 5000 - 0 for control and concentration of 12.5-500 nM, and 10000 - 0 for concentrations of 1 and 10 µM; B) 5000 - 0 for control and concentrations of 12.5-300 nM, and 10000 - 0 for concentrations of 500 nM-10 µM.

Integration analysis delivers information about distribution of selected compounds, whereas cluster analysis is useful especially to study the composition of complex samples. As a result of k-means cluster analysis (KMCA) average spectra and chemical maps of all components present in the sample were obtained. To show that accumulation of DOX and DNR within cell nuclei is varied the KMC analysis in the 500-1800 cm^{-1} range using the Manhattan distance and 5 main chemical cluster was provided (Figure 4).
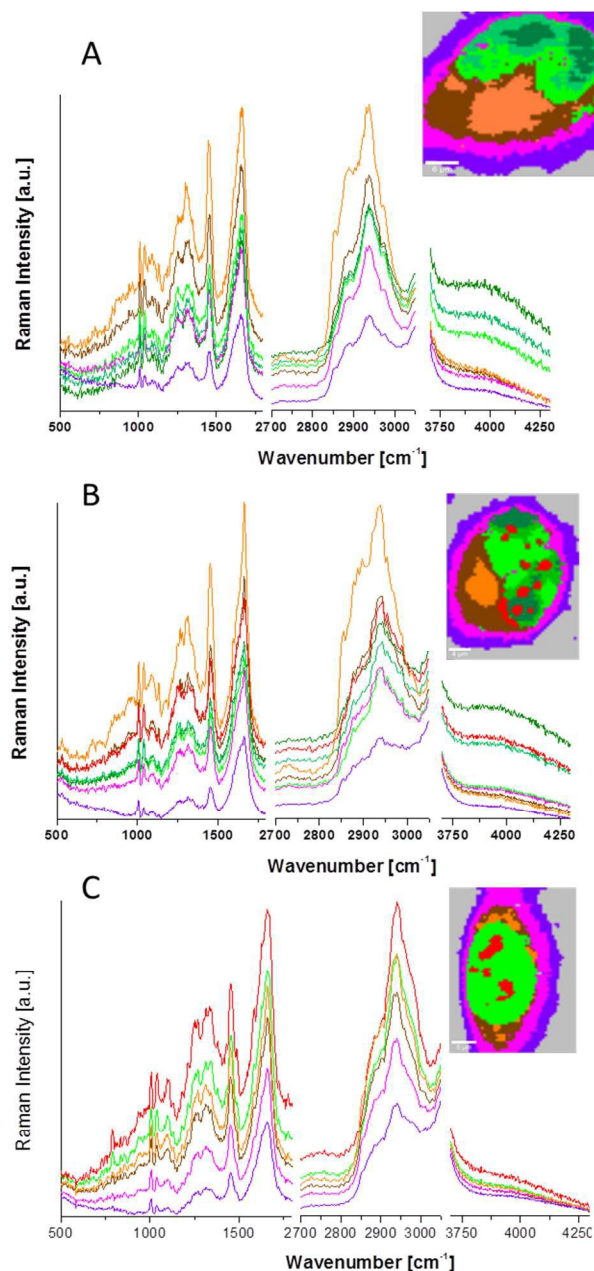
Figure 4 Cluster maps of EA.hy 926 cells (incubated with 10 µM DNR or DOX and control) obtained by the application of K-means analysis with the average spectra of clusters (green – nucleolus; red – nucleoli; brown – mixture of cytoplasm and small organelles; orange – lipid rich small organelles, e.g. endoplasmic reticulum; magenta – cytoplasm, violet – mostly cell membrane with cytoplasm and adhesion proteins).

Different tones of green color were used for coding different areas of cell nuclei. Dark green correlates with a significant increase of the background in the 3820-4245 cm^{-1} spectral range that suggests that this area is rich in anthracycline antibiotics. Lower concentration of DNR and DOX is coded using middle intense green color, however bright green areas were relatively poor (Figure 4A) in anthracycline or even anthracycline free (Figure 4B). For control cells KMC analysis did not provide any variation in the nucleus.

Differences in intensity in nuclear accumulation i.e. different intensity of the background above 3800 cm^{-1} can be related to

distribution of eu- and heterochromatin (transcriptionally active and no active regions, respectively).

A similar analysis as for the DOX and DNR was performed for epimers of these compounds (Figure 5). Examples of chemical maps obtained by the integration of the Raman spectra in the 2800–3020, 775–810 and 3820-4245 cm^{-1} spectral ranges show the distribution of selected compounds. Accumulated antibiotics within the nucleus of cells can be also observed using high spectral range.
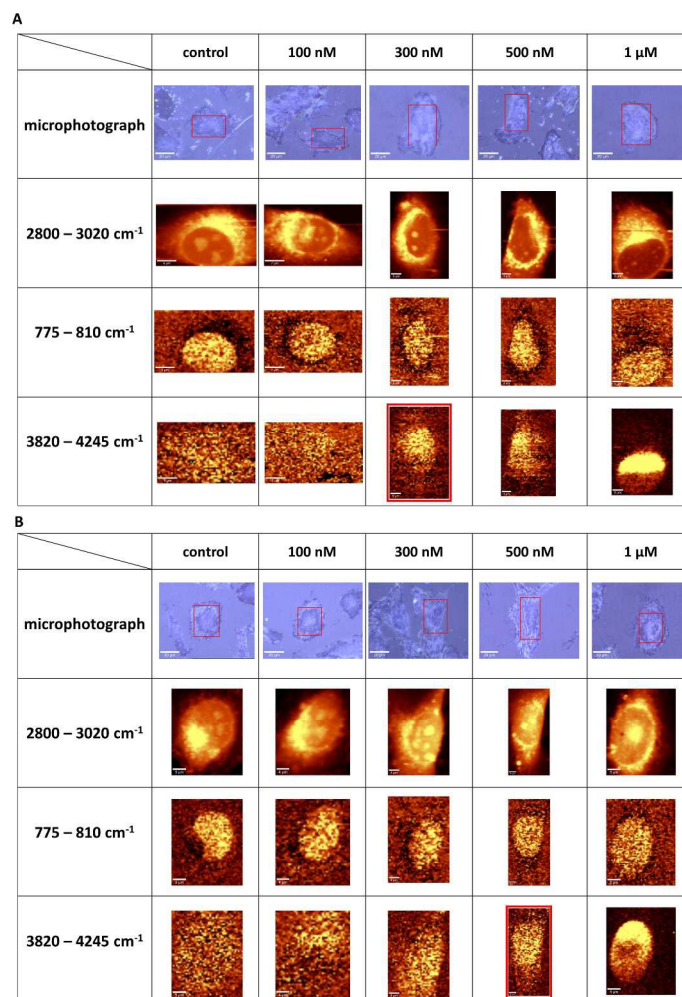

Figure 5 Examples of chemical maps obtained by the integration of the Raman spectra over the ν_{C-H} band (2800–3020 cm^{-1}), cytosine ring vibration of DNA (775–810 cm^{-1}) and 3820-4245 cm^{-1} (spectral range of anthracycline antibiotic maximum fluorescence). A – Integration maps and microphotographs of epidoxorubicin (EDOX) treated endothelium, B – integration maps and microphotographs of epidaunorubicin (EDNR)-treated endothelium. Results for all investigated concentrations of anthracycline antibiotic are shown. Scale bar for bottom row: A) 8000 - 0 for control and concentrations of 100-500 nM, and 20000 - 0 for concentration of 1 µM; B) 6000 - 0 for control and concentrations of 100-500 nM, and 15000 - 0 for concentration of 1 µM.

Raman mappings followed by an observation of antibiotics' fluorescence in the high wavenumber range indicated that EDOX in concentrations of 300 nM and higher and EDNR in concentrations of 500 nM and higher was easily detected in nuclei of endothelial cells.

Difference in chemical structure between DOX, DNR and their epimers is subtle and for DOX vs EDOX and DNR vs EDNR is

related to changes in configuration of the hydroxyl group at the 4' position (Figure 1). EDOX is known to be less cardiotoxic than DOX in both acute and chronic toxicity studies but there is no clear-cut difference in tumour response rate or tumour-bearing mice survival treated with epirubicin or doxorubicin.[31,39] Results presented in this work indicate similar nuclear accumulation of DOX and EDOX in the endothelial cells. Both agents were detected in the nucleus at the similar range of concentrations (DOX demonstrates only slightly stronger nuclear accumulation but the "threshold concentrations" for both compounds was around 300 nM)). Interestingly, in the case of DNR and EDNR results were significantly different. The lowest concentration at which DNR was detected within the nucleus was 50 nM, while for EDNR the threshold concentration was approximately 10 times higher and amounted to 500 nM. These results suggest that EDNR display much lower ability to accumulate in the nucleus of endothelial cells as compared to DNR.
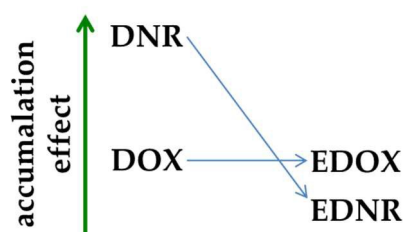

Figure 6 A schematic comparison of nuclear accumulation of epimers as compared to their congeners DOX and DNR based on spectroscopic results presented in Figure 3 and 5.

In brief, the nuclear accumulation of EDOX did not really differed with that for DOX, while DNR accumulation was much more pronounced than that of EDNR despite the fact that modification of chemical structure in epimers of DOX and DNR is the same and entails only different position of hydroxyl group at the 4' position. The scheme depicting the obtained results in a schematic way is presented in Figure 6.
In the present work we also investigated the nuclear accumulation of anthracyclines using high-content fluorescence microscopy Staining with Hoechst 33342 to detect nuclear area for anthracycline accumulation.
Figure 7A shows comparison of nuclear fluorescence for DNR and EDNR (calculated as a percent of control) detected in nucleus in concentrations higher than 300 nM and higher than 500 nM for DNR and EDNR, respectively. In case of DOX and its epimer fluorescence of the drug was detected in nucleus at a similar concentration (Figure 7B). Even though the tendency for differential nuclear accumulation for EDNR vs DNR was confirmed as well as similar accumulation for EDOX vs DOX using high-content fluorescence microscopy results are not so explicit as in the case of Raman microspectroscopy. These results suggest clear-cut advantage of Raman spectroscopy as a more sensitive tool to detect anthracyclin nuclear accumulation allowing also to investigate changes in biochemical composition of the cell subjected to anthracycline treatment.
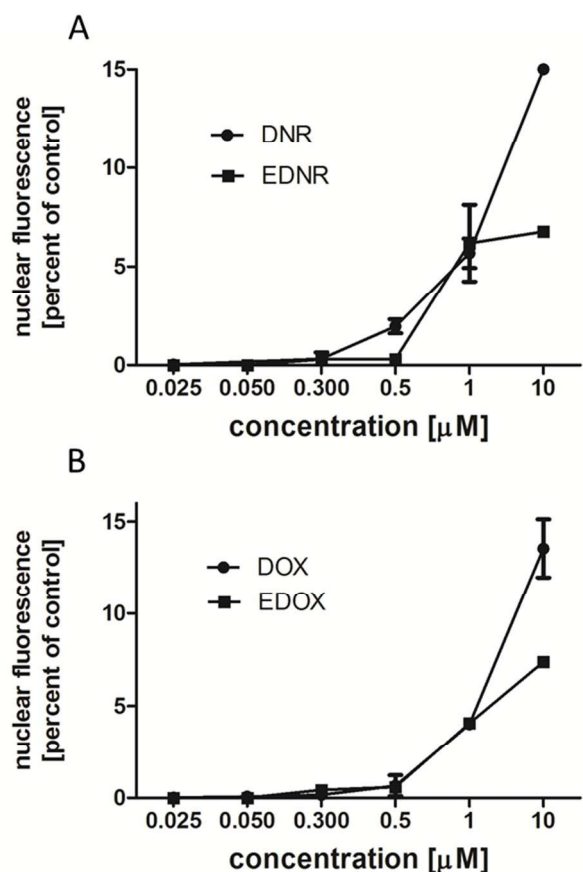
Figure 7 High-content fluorescence microscopy results for individual cells presented as means and standard deviations (SD). A - comparison of nuclear fluorescence for DNR and EDNR (calculated as a percent of control), B - comparison of nuclear fluorescence for DOX and EDOX.

The most surprising finding of this work was that nuclear accumulation of four studies anthracycline did not relate to their toxicity. Based on MTT results DNR caused a loss in cells metabolic activity at lower concentrations (IC50 [μM] $\pm$ SEM around 0.7080 ± 0.4394) than DOX (IC50 [μM] $\pm$ SEM around 1.138 ± 0.6145). MTT results for EDOX suggest lower loss in cells metabolic activity for EDOX (IC50 [μM] $\pm$ SEM around 2.891 ± 0.5926) as compared to DOX. While MTT results for DNR and EDNR were as follows: (IC50 [μM] $\pm$ SEM around 0.7080 ± 0.4394 and 1.144 ± 0.4417, respectively.
Effects of DOX, DNR and their epimers on caspases 3 and 7 activities are presented in Figure 8.
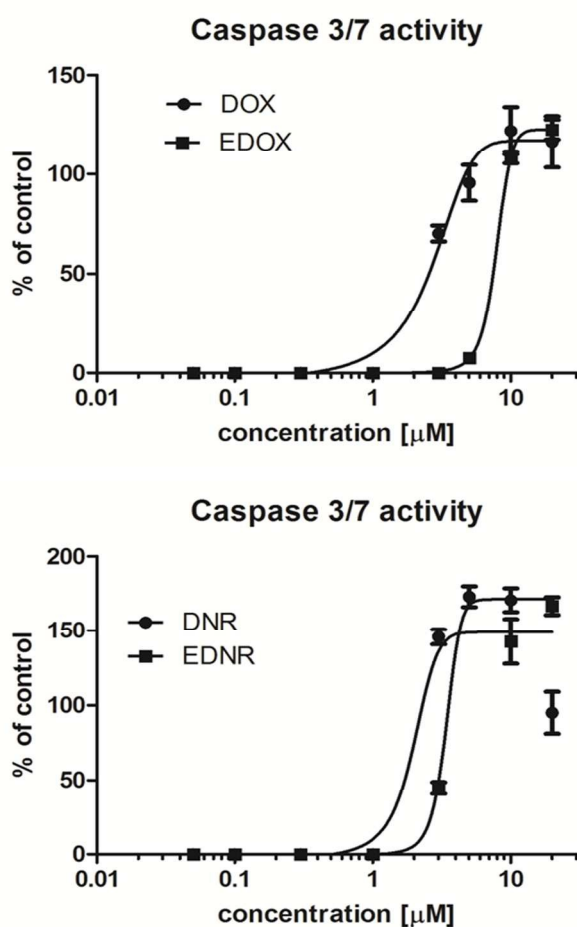
Figure 8 Results of caspases 3 and 7 assay. DNR at concentrations >1 µM and DOX at concentrations >2 µM induced significant activation of caspases 3 and 7, clearly suggesting that the cells undergo changes leading to programmed cells death.

DNR at concentrations >1 µM and DOX at concentrations >2 µM induced significant activation of caspases 3 and 7, clearly suggesting that the cells undergo changes leading to programmed cells death and their respective epimers were weaker to induce activation of caspases 3 and 7.

To examine effects of DOX, DNR and their respective epimers on the ability of endothelial cells to migration and proliferation, an automated wound healing assay with Electric Cell-substrate Impedance Sensing (ECIS) was applied. ECIS is a real-time, label-free, and impedance-based method to study the activities of cells grown in the culture. It allows investigation of morphological changes, cell locomotion, and other behaviors directed by the cell's cytoskeleton[40]. After the cells were added to the ECIS arrays they attach to the electrodes and act as insulators increasing the impedance. When cells were confluent at the electrodes, the current is impeded in a manner related to the number of cells covering the electrode, the morphology of the cells and the nature of the cell attachment. When cells are stimulated to change their function, the accompanying changes in cell morphology alter the impedance.[41] The results obtained using ECIS assay are shown in Figure 9.
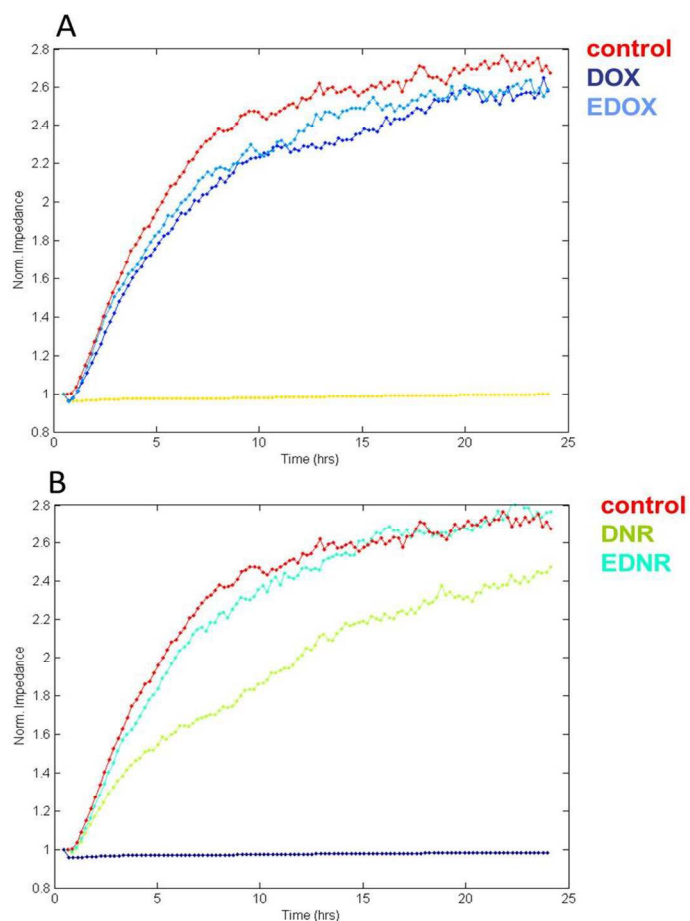
Figure 9 A representative results of an automated wound healing assay with Electric Cell-substrate Impedance Sensing (ECIS). The rate of cells migration to wounded area was diminish for cells treated with anthracyclines, comparing to control. For DOX (A, dark blue line) the effect was more pronounced, than for its epimer EDOX (A, light blue line). Similarly for DNR (B, light green line) and its epimer (B, blue-green line).

The rate of cells migration to wounded area was diminish for cells treated with anthracyclines, in comparison to the control. For DOX (Figure 9A, dark blue line) the effect seem to be slightly more pronounced than for its epimer EDOX (Figure 9A, light blue line). For DNR (Figure 9B, light green line) the effect was substantially more pronounced then for its epimer (Figure 9B, blue-green line).

Conclusions

Clinical usefulness of anthracyclines antibiotics is imitated by their cardiovascular and vascular toxicity that could be linked to the genotoxic effects of these compounds. In the present work we aimed to develop bimodal Raman and fluorescence-based methodology to study relationship between nuclear accumulation of anthracycline and their endothelial toxicity. We compared nuclear accumulation of structurally-related anthracyclines (DOX, DNR) and their epimers (EDOX, EDNR) in endothelium and demonstrated that accumulation of DOX and DNR in nucleus was observed in nanomolar range of concentrations what is close to range of drug concentration in

plasma of patients treated with doxorubicin and daunorubicin. Raman based microspectroscopy allowed for subcellular analysis of organelles in relation to the anthracycline localization. These results suggest that bimodal, Raman and fluorescence imaging could be regarded as a valuable tool to study endothelial toxicity of anthracyclines. Interestingly, we showed that DNR epimer but not DOX epimer accumulated to a lesser extent in the endothelial nucleus, while both epimers were less toxic as compared to their DOX and DNR counterparts. Accordingly, accumulation in nucleus did not seem to correlate directly with their toxicity. These results suggest that non-nuclear mechanisms of toxicity or distinct nuclear transport for respective epimers might be contribute to the endothelial mechanisms of toxicity of these compounds.

Acknowledgements

Notes

[a] Faculty of Chemistry, Jagiellonian University, Ingardena 3, Krakow, Poland.

[b] Jagiellonian Centre for Experimental Therapeutics (JCET), Jagiellonian University, Krakow, Poland.

[c] Institute of Biotechnology and Antibiotics, Staroscinska 5, 02-516 Warsaw, Poland.

[d] Department of Experimental Pharmacology, Chair of Pharmacology, Jagiellonian University, Medical College, Grzegorzecka 16, Krakow, Poland.

Correspondence:baranska@chemia.uj.edu.pl;stefan.chlopicki@jcet.eu

*These authors are senior authors of this work.

References

1. C. Krafft, T. Knetschke, R. H. W. Funk, and R. Salzer, *Anal. Chem.*, 2006, **78**, 4424–9.
2. T. J. Harvey, E. C. Faria, A. Henderson, E. Gazi, A. D. Ward, N. W. Clarke, M. D. Brown, R. D. Snook, and P. Gardner, *J. Biomed. Opt.*, 2008, **13**, (064004) 1–12.
3. X. L. Yan, R. X. Dong, L. Zhang, X. J. Zhang, and Z. W. Zhang, *World J Gastroenterol*, 2005, **11**, 3290–2.
4. A. V. Feofanov, A. I. Grichine, L. A. Shitova, T. A. Karmakova, R. I. Yakubovskaya, M. Egret-Charlier, and P. Vigny, *Biophys. J.*, 2000, **78**, 499–512.
5. J. Guo, W. Cai, B. Du, M. Qian, and Z. Sun, *Biophys. Chem.*, 2009, **140**, 57–61.
6. H. Yao, Z. Tao, M. Ai, L. Peng, G. Wang, B. He, and Y. Li, *Vib. Spectrosc.*, 2009, **50**, 193–197.
7. C. Matthäus, T. Chernenko, J. A. Newmark, C. M. Warner, and M. Diem, *Biophys. J.*, 2007, **93**, 668–73.
8. C. Krafft, T. Knetschke, R. H. W. Funk, and R. Salzer, *Vib. Spectrosc.*, 2005, **38**, 85–93.
9. G. J. Puppels, H. S. Garritsen, J. A. Kummer, and J. Greve, *Cytometry*, 1993, **14**, 251–6.
10. F. Bonnier, P. Knief, B. Lim, a D. Meade, J. Dorney, K. Bhattacharya, F. M. Lyng, and H. J. Byrne, *Analyst*, 2010, **135**, 3169–77.
11. R. Manoharan, Y. Wang, and M. S. Feld, *Spectrochim. Acta Part A Mol. Biomol. Spectrosc.*, 1996, **52**, 215–249.
12. M. Gniadecka, H. C. Wulf, and N. N. Mortensen, *J. Raman Spectrosc.*, 1997, **28**, 125–129.
13. M. Moreno, L. Raniero, E. Â. L. Arisawa, A. M. Espírito Santo, E. A. P. Santos, R. A. Bitar, and A. A. Martin, *Theor. Chem. Acc.*, 2009, **125**, 329–334.
14. C. Scalfi-Happ, A. Jauss, W. Ibach, O. Hollricher, S. Fulda, C. Hauser, R. Steiner, and A. Rück, *Med. Laser Appl.*, 2007, **22**, 157–164.
15. M. B. Fenn, P. Xanthopoulos, G. Pyrgiotakis, S. R. Grobmyer, P. M. Pardalos, and L. L. Hench, *Adv. Opt. Technol.*, 2011, **2011**, 1–20.
16. M. S. Bergholt, W. Zheng, K. Lin, K. Y. Ho, M. Teh, K. G. Yeoh, J. B. Yan So, and Z. Huang, *Int J Cancer*, 2011, **128**, 2673–80.
17. K. W. Short, S. Carpenter, J. P. Freyer, and J. R. Mourant, *Biophys. J.*, 2005, **88**, 4274–88.
18. C. Kendall, M. Isabelle, F. Bazant-Hegemark, J. Hutchings, L. Orr, J. Babrah, R. Baker, and N. Stone, *Analyst*, 2009, **134**, 1029–45.
19. J. Choi, J. Choo, H. Chung, D.-G. Gweon, J. Park, H. J. Kim, S. Park, and C.-H. Oh, *Biopolymers*, 2005, **77**, 264–72.
20. C. Krafft and V. Sergo, *Spectroscopy*, 2006, **20**, 195–218.
21. S. K. Teh, W. Zheng, K. Y. Ho, M. Teh, K. G. Yeoh, and Z. Huang, *Br. J. Cancer*, 2008, **98**, 457–65.
22. C. Krafft, G. Steiner, C. Beleites, and R. Salzer, *J. Biophotonics*, 2009, **2**, 13–28.
23. A. T. Harris, A. Rennie, H. Waqar-Uddin, S. R. Wheatley, S. K. Ghosh, D. P. Martin-Hirsch, S. E. Fisher, A. S. High, J. Kirkham, and T. Upile, *Head Neck Oncol.*, 2010, **2**, 26.
24. K. Majzner, K. Kochan, N. Kachamakova-Trojanowska, E. Maslak, S. Chlopicki, and M. Baranska, *Anal. Chem.*, 2014, **86**, 6666–74.
25. C. Matthäus, T. Chernenko, L. Quintero, L. Milan, A. Kale, M. Amiji, V. Torchilin, and M. Diem, in *Proc. of SPIE 6991*, eds. J. Popp, W. Drexler, V. V. Tuchin, and D. L. Matthews, 2008, vol. 6991, p. (699106) 1–8.
26. H. Nawaz, F. Bonnier, P. Knief, O. Howe, F. M. Lyng, A. D. Meade, and H. J. Byrne, *Analyst*, 2010, **135**, 3070–6.
27. R. B. Weiss, *Semin. Oncol.*, 1992, **19**, 670–86.
28. M. Wasowska, I. Oszczapowicz, J. Wietrzyk, A. Opolski, J. Madej, S. Dzimira, and J. Oszczapowicz, *Anticancer Res.*, **25**, 2043–8.
29. E. Ciesielska, K. Studzian, M. Wasowska, I. Oszczapowicz, and L. Szmigiero, *Cell Biol. Toxicol.*, **21**, 139–47.
30. H. Cortés-Funes and C. Coronado, *Cardiovasc. Toxicol.*, 2007, **7**, 56–60.
31. L. A. Smith, V. R. Cornelius, C. J. Plummer, G. Levitt, M. Verrill, P. Canney, and A. Jones, *BMC Cancer*, 2010, **10**, 337.
32. J. B. Chaires, J. E. Herrera, and M. J. Waring, *Biochemistry*, 1990, **29**, 6145–53.
33. V. Cassina, D. Seruggia, G. L. Beretta, D. Salerno, D. Brogioli, S. Manzini, F. Zunino, and F. Mantegazza, *Eur. Biophys. J.*, 2011, **40**, 59–68.
34. J. B. Chaires, K. R. Fox, J. E. Herrera, M. Britt, and M. J. Waring, *Biochemistry*, 1987, **26**, 8227–8236.
35. J. B. Chaires, *Biopolymers*, 1997, **44**, 201–15.
36. I. R. Nabiev, H. Morjani, and M. Manfait, *Eur. Biophys. J.*, 1991, **19**, 311–6.
37. M. A. Ivi, S. D. Petrovi, E. Kalmán, T. Milosavljevi, and I. Reljin, 2005, **70**, 823–831.
38. T. Wojcik;, E. Buczek;, K. Majzner;, A. Kolodziejczyk;, J. Miszczyk;, W. Kwiatek;, M. Baranska;, M. Szymonski;, and S. Chlopicki, *Toxicol. Vitr.*
39. S. Toldo, R. W. Goehe, M. Lotrionte, E. Mezzaroma, E. T. Sumner, G. G. L. Biondi-Zoccai, I. M. Seropian, B. W. Van Tassell, F. Loperfido, G. Palazzoni, N. F. Voelkel, A. Abbate, and D. a Gewirtz, *PLoS One*, 2013, **8**, e58421.
40. J. Wegener, C. R. Keese, and I. Giaever, *Exp. Cell Res.*, 2000, **259**, 158–66.
41. C. R. Keese, J. Wegener, S. R. Walker, and I. Giaever, *Proc. Natl. Acad. Sci. U. S. A.*, 2004, **101**, 1554–9.